Structural and Kinetic Studies on the Potent Inhibition of Metallo-β-Lactamases by 6-Phosphonomethylpyridine-2-Carboxylates

Philip Hinchliffe[1,$], Carol A. Tanner[2,$], Anthony P. Krismanich[2], Geneviève Labbé[2], Valerie J. Goodfellow[2], Laura Marrone[2], Ahmed Y. Desoky[2], Karina Calvopiña[1], Emily E. Whittle[1], Fanxing Zeng[3], Matthew B. Avison[1], Niels C. Bols[3], Stefan Siemann[4], James Spencer[1,], Gary I. Dmitrienko[2,5,*]*

[$]equal contribution

[*]co-corresponding

[1]School of Cellular & Molecular Medicine, University of Bristol, Bristol BS8 1TD, UK.

[2]Department of Chemistry, University of Waterloo, Waterloo, Ontario, Canada, N2L 3G1.

[3]Department of Biology, University of Waterloo, Waterloo, Ontario, Canada, N2L 3G1

[4]Department of Chemistry and Biochemistry, Laurentian University, Sudbury, Ontario, Canada, P3E 2C6

[5]School of Pharmacy, University of Waterloo, Waterloo, Ontario, Canada, N2L 3G1

*Corresponding authors

Gary. I. Dmitrienko, e-mail: dmitrien@uwaterloo.ca

James Spencer, e-mail: jim.spencer@bristol.ac.uk

Author contributions: P.H., C.A.T., A.P.K., G.L., V.J.G., L.M., A.Y.D., K.C., E.E.W., F.Z., performed the experiments; all authors analysed data; P.H., C.A.T., G.L., M.B.A., N.C.B., S.S., J.S., G.I.D., designed research; P.H., J.S., G.I.D., wrote the paper.

Abstract

There are currently no clinically available inhibitors of metallo-β-lactamases (MBLs), enzymes which hydrolyze β-lactam antibiotics and confer resistance on Gram-negative bacteria. Here we present 6-phosphonomethylpyridine-2-carboxylates (PMPCs) as potent inhibitors of subclass B1 (IMP-1, VIM-2, NDM-1) and B3 (L1) MBLs. Inhibition followed a competitive, slow-binding model without an isomerization step (IC$_{50}$ values $0.3 - 7.2$ µM; K_i $0.03 - 1.5$ µM). Minimum inhibitory concentration assays demonstrated potentiation of β-lactam (meropenem) activity against MBL-producing bacteria, including clinical isolates, at concentrations where eukaryotic cells remain viable. Crystal structures revealed unprecedented modes of inhibitor binding to B1 (IMP-1) and B3 (L1) MBLs. In IMP-1, binding does not replace the nucleophilic hydroxide and the PMPC carboxylate and pyridine nitrogen interact closely (2.3 and 2.7 Å, respectively) with the Zn2 ion of the binuclear metal site. The phosphonate group makes limited interactions, but is 2.6 Å from the nucleophilic hydroxide. Furthermore, the presence of a water molecule interacting with the PMPC phosphonate and pyridine N-C2 π-bond, as well as the nucleophilic hydroxide, suggests that the PMPC binds to the MBL active site as its hydrate. Binding is markedly different in L1, with the phosphonate displacing both Zn2, forming a monozinc enzyme, and the nucleophilic hydroxide, while also making multiple interactions with the protein main chain and Zn1. The carboxylate and pyridine nitrogen interact with Ser221/223, respectively (3 Å distance). The potency, low toxicity, cellular activity and amenability to further modification of PMPCs indicate these and similar phosphonate compounds can be further considered for future MBL inhibitor development.

Introduction

Antibacterial drug resistance is an increasingly major clinical problem, particularly due to the reduced efficacy of β-lactam antibiotics against Gram-negative pathogens such as *Escherichia coli*, *Klebsiella pneumoniae, Pseudomonas aeruginosa* and *Stenotrophomonas maltophilia*.[1, 2] β-lactams remain key agents for treatment of Gram-negative infections, with the carbapenems and third generation cephalosporins being the first choice chemotherapeutic agents. Among the major resistance determinants are zinc-dependent metallo-β-lactamases (MBLs), zinc-dependent enzymes which hydrolyze almost all β-lactams including the carbapenems and cephalosporins.[1-6] MBLs all have a similar overall fold with the active site lying in a groove formed by two beta sheets, but are subdivided into three subclasses (B1, B2 and B3) based on sequence, structure and the number of zinc ions in their active site.[7-10] In B1 and B3 MBLs, the active site contains two zinc ions, Zn1 coordinated by His116, His118 and His196 (standard MBL numbering scheme[8] used throughout) and Zn2 by Asp120, His263 and either Cys221 in the B1 or His121 in the B3 subclasses. A water/hydroxide bridges/coordinates the two zinc ions, and is thereby potentially activated to act as a nucleophile to attack the β-lactam ring.[10] By comparison, subclass B2 MBLs are active as monozinc enymes, with the single zinc ion coordinated by Asp120, Cys221 and His263 in a similar architecture to the Zn2 site in B1 MBLs.[11] In contrast to the serine-β-lactamases (SBLs)[12] there are currently no clinically useful MBL inhibitors. The differences between the various MBL active sites have hindered the development of inhibitors active against all MBLs.

MBL inhibitor design has focused on compounds that include metal binding moieties such as nitrogen, thiols and carboxylates or compounds which mimic hydrolysis intermediates, such as the bicyclic boronates.[13] The various thiols are the best studied, with captopril, a molecule containing both a thiol and carboxylate group, as the most prominent example. The D- and L-stereoisomers of captopril are variously effective against B1 and B3 MBLs with IC$_{50}$'s covering a wide range, from 0.072 µM to over 500 µM, depending on the captopril stereoisomer and MBL variant.[14] X-ray crystal structures show the thiol group bridges the two active site zinc ions of B1 and B3 MBLs, while in B2 MBLs the carboxylate interacts with the Zn2 site,[15] with the thiol group uninvolved. More recently we described bisthiazolidines[16-18] which contain not only a thiol group but also nitrogen and carboxylate moieties, and can inhibit B1 enzymes such as NDM-1 (*in vivo* IC$_{50}$ 23-201 µM), again through a zinc-bridging thiol group. The carboxylate group of both captoprils and bisthiazolidines can also interact with residues on the protein main chain (Lys224 or Ser221 in B1 and B3 enzymes, respectively) that have

previously been shown to bind hydrolyzed substrate.[19, 20] A number of other crystal structures of thiols bound to MBLs show similar binding modes, with the thiol bridging the two zincs in B1[21-24] and B3[15, 25, 26] MBLs, and a carboxylate[15] or the thiol[27] binding to the monozinc center of B2 MBLs.

The binding modes of potent (IC_{50} values ranging between 0.003 μM and 7 μM[13]) dicarboxylate MBL inhibitors are also well understood, with crystal structures available of such compounds bound to all three MBL subclasses: biaryl succinic acid[28] and 3-aminopthalic acid[29] to the B1 enzyme IMP-1, 2,4 pyridine dicarboxylic acid to *Aeromonas hydrophila* CphA (B2)[30], and furan/pyrazole-constrained dicarboxylic acids to *S. maltophilia* L1 (B3)[26]. In all cases, binding is similar to that of thiols, with one carboxylate moiety bridging the two active site zinc ions, and the second carboxylate interacting with a Ser or Lys residue. In the case of dicarboxylate inhibition of the B2 MBL CphA, only one of the two carboxylates is involved in active site interactions, binding the zinc ion, although the nitrogen of the pyridine ring also ligands the zinc ion. Nitrogen-based inhibition, by tetrazole-based ligands (IC_{50} ~18-300 μM[28]) and 4-nitrobenzene-sulfonamide (IC_{50} not reported), has also been structurally characterized in B1 (*Bacteroides fragilis* CcrA[31]) and B3 (*Bradyrhizobium japonicum* BJP-1[32]) MBLs. In both cases, inhibition is achieved by interaction of an inhibitor-nitrogen with either the Zn2 site only (CcrA) or both Zn1 and Zn2 (BJP-1).

Bicyclic boronates are proposed to mimic the tetrahedral oxyanion formed during β-lactam hydrolysis.[33] They inhibit B1 enzymes ($IC50s$ 0.003 – 1 μM) through interaction of the 'exocyclic' boronate oxygen within the dizinc center, displacing the nucleophilic hydroxide, and the 'endocylic' boronate ester oxygen with Zn2. As with other inhibitors, the carboxylate interacts with both Zn2 and Lys224 (e.g. NDM-1) or Arg228 (e.g. VIM-2) on the protein main chain. The bicyclic boronates do not inhibit the B3 enzymes, such as *S. maltophilia* L1.[34]

Less well understood is MBL inhibition by compounds containing phosphonate, a moiety well known to chelate zinc and inhibit metalloenzymes.[35-37] In addition, phosphonate monoesters have been shown to inhibit SBLs by formation of a tetrahedral intermediate-mimic covalently bound to the active-site serine.[38, 39] Mercaptophosphonate compounds, which contain both a phosphonate and thiol group, have been reported as competitive inhibitors of all MBL classes, with K_i values from 0.4 to over 400 μM.[27] Indeed, in the crystal structure of a mercaptophosphonate:B2 CphA complex the phosphonate preferentially binds the zinc ion over the thiol group.[27] There is potential of phosphonates to act as analogues of mechanistically

important oxyanionic species in MBL-catalyzed β-lactam hydrolysis. A recent study on a β-phospholactam (containing a cyclic phosphonamidate, that might undergo hydrolysis to a phosphonate in aqueous medium) exhibited modest time-dependent inhibition of B1 and B3 MBLs at 100 µM.[40] However, to date the utility of phosphonates as broad-spectrum inhibitors active against multiple MBL subclasses remains underexplored. Accordingly, here we investigate phosphonate-based pyridine-carboxylates (PMPCs, **Figure 1**) as inhibitors of clinically relevant B1 and B3 MBLs. Our data show that these compounds inhibit a range of MBL targets and, through X-ray crystallography and kinetic experiments, define their mode of binding to, and mechanism of inhibition of, target B1 and B3 MBLs. Importantly, we also demonstrate potentiation of β-lactam antibacterial activity against both laboratory and clinical strains of MBL-producing bacteria, suggesting that these compounds may be useful against medically-relevant antibiotic resistant pathogens.
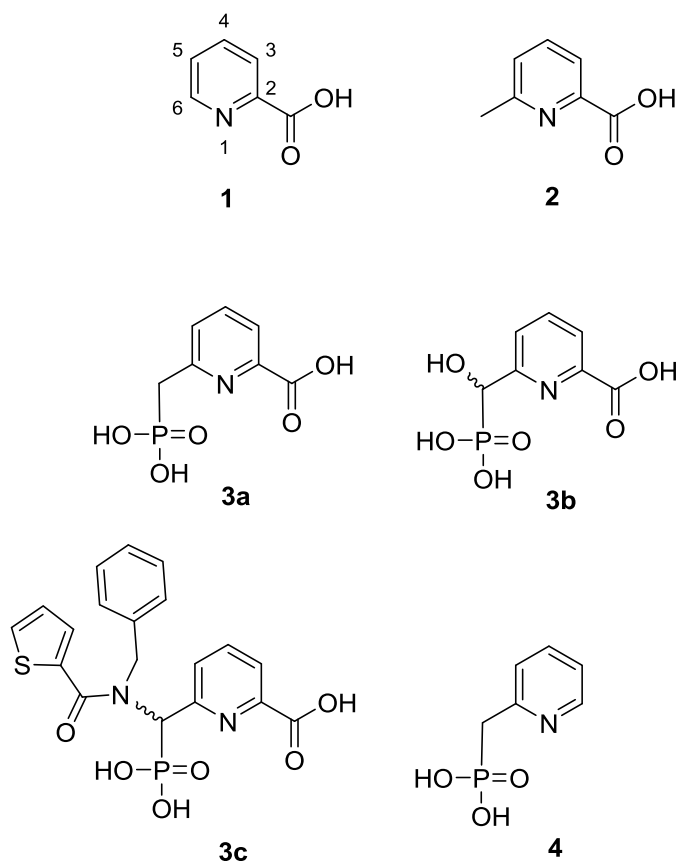
Figure 1. Structures of pyridine-2-carboxylates used in this study. 1, PA, 2-picolinic acid; **2,** MPA, 6-methylpicolinic acid; **3a**, PMPC-1, 6-(phosphonomethyl)pyridine-2-carboxylate; **3b,** PMPC-2, 6-[hydroxy(phosphono)methyl]picolinic acid; **3c**, PMPC-3, 6-[(N-benzyl-1-thiophen-2-ylformamido)(phosphono)methyl]picolinic acid; **4**, (pyridin-2-ylmethyl)phosphonic acid.

Materials and Methods

Materials

All reagent chemicals used in synthesis, including 2-picolinic acid (**1**) and 6-methyl-2-picolinic acid (**2**), were acquired from Sigma-Aldrich (Canada) and were employed as received. Nitrocefin was obtained from Oxoid or prepared synthetically as described previously.[41]

Inhibitor synthesis

The synthesis and characterization of PMPC-1 (**3a**) has been reported previously.[42] The synthesis and spectroscopic characterization of PMPC-2 (**3b**), PMPC-3 (**3c**) and PMP (**4**) is described in Electronic Supplementary Information (ESI).

Minimum Inhibitory Concentration assays

Bacterial Strains/Plasmids: Open reading frames, together with the associated promoter sequences, encoding the IMP-1, VIM-1 and NDM-1 MBLs were amplified from clinical samples by PCR and cloned into the pSU18 broad host range vector as previously described.[33, 43] *E. coli* MG1655, *K. pneumoniae* Ecl8, *Citrobacter freundii* and *Enterobacter aerogenes* were transformed with the resulting plasmids by electroporation. *K. pneumoniae* strain UWB116 (N11-2218) (as recently employed in a study of the natural product aspergillomarasmine A[44]) was a generous gift from Dr. A. McGeer at Mount Sinai Hospital, Toronto. *P. aeruginosa* strain UWB41 (IS6654) and *S. maltophilia* strain UWB26 (IS5563) are meropenem-resistant strains kindly provided by Dr. Dylan Pillai from the collection of clinical isolates maintained at the Ontario Agency for Health Protection and Promotion (now known as Public Health Ontario) in Toronto, Ontario. *P. aeruginosa* strain UWB78 (VIM-I-1; 03-RL-03-2453), *P. putida* strain UWB24 (C10; PS679/00), *E. coli* strain UWB75 (MH1-NDM-1) and *E. coli* strain UWB93 (Ec7-IMP) originated from the collection of clinical isolates maintained at Calgary Laboratory Services, Calgary, Alberta and were kindly provided by Dr. Johann Pitout and Dr. Dylan Pillai. *S. maltophilia* strains K279a, K ami32 (efflux pump overproducing mutant) and JKWZP (knock-out strain lacking the RND pumps SmeJ/K/W/Z/P) were described previously.[45-47] For all strains species identification and presence of specific MBLs was confirmed by PCR using 16S rDNA and MBL-specific primers, respectively.

Minimum Inhibitory Concentration (MIC) Determination: MIC values were determined by broth microdilution, in triplicate, in cation adjusted Mueller Hinton broth (Sigma) according to the Clinical Laboratory Standards Institute (CLSI) guidelines.[48] Experiments were carried out

6

in microtiter plates (Corning) containing the medium plus meropenem and inhibitor (dissolved in DMSO) as appropriate. Plates were incubated overnight at 37 °C for 18 – 24 h and absorbance at 600 nm read using Polarstar Omega (BMG LabTech) or Powerwave XS2 (Biotek) plate readers.

Cell toxicity assay

Cell culture: The mammalian cell lines were the rat liver hepatoma cell line H4IIE (ATCC Accession No. CRL-1600) and two human cell lines, Caco2, a colon adenocarcinoma cell line (ATCC Accession No. HTB-37), and HepG2, a liver hepatoma cell line (ATCC Accession No. CRL- 11997). Cells were routinely cultured in Dulbecco's Modified Eagle's Medium (DMEM, Sigma) supplemented with 10% fetal bovine serum (FBS) in 75-cm^2 vented culture flasks at 37 ºC in a humidified 5% CO_2 atmosphere.

Plating and dosing: Cells were seeded in 96 well plates (Becton and Dickinson Company, Franklin Lakes, NJ. USA) at a density of 4×10^4 cells per well in 200 µl of DMEM growing medium with 10% FBS supplement. Cells were allowed to settle and reattach for 24 h at room temperature before being exposed to any compounds. The cells were then dosed with varying concentrations of **3a** in DMEM without 10% FBS. Application of chemicals to cell cultures was done by adding culture medium mixed with chemical solution to the culture well. The final concentration of the solvents (such as DMSO or water) in each well was the same as for the control wells, which were only dosed with solvent. After 24 h, cultures were evaluated for cytotoxicity. In no cases was the solvent used at a concentration that was cytotoxic.

Measuring cell viability: Three fluorescent indicator dyes were used to evaluate cell viability.[49, 50] Metabolic activity was measured by Alamar Blue (Medicorp, Montreal, PQ). Cell membrane integrity was evaluated with 5-carboxyfluorescein diacetate (CFDA-AM) (Molecular Probes, Eugene, OR). Lysosome integrity was monitored with Neutral Red (Sigma-Aldrich). Alamar Blue, CFDA-AM and Neutral Red were prepared in Dulbecco's phosphate buffered saline (DPBS, Lonza, Walkersville, MD USA) to give final concentrations of 5% (v/v), 4 µM and 1.5% (v/v) respectively. Cells were incubated with dyes for 1 h in dark, then quantified by fluorescence plate reader (Spectra-max Gemini XS microplate spectrofluorometer; Molecular Devices, Sunnyvale, CA). The excitation band emission wave-lengths used were 530 and 590 nm for Alamar Blue, 485 and 530 nm for CFDA-AM, 530 and 640 nm for Neutral Red, respectively. Results were calculated as a percent of the control culture.

7

Data analysis: All graphs and statistical analyses were done using GraphPad InStat (version 4.01 for Windows XP, GraphPad Software, San Diego, CA, www.graphpad.com).

Protein purification

NDM-1, VIM-2, IMP-1 and L1 were purified as previously described.[18, 51-53]

Enzyme Kinetics

All data analysis of enyme kinetics was performed using GraphPad Prism version 5.00 for Windows (GraphPad Software, San Diego California USA, www.graphpad.com).

IC$_{50}$ Assays: Inhibitor stocks were prepared by dissolving the PMPC compound in 100% DMSO to a final concentration of 100 mM. Compound PMP stocks were prepared as 50 mM compound in 50 mM HEPES pH 7.2.

Enzyme (IMP-1, 186 pM; VIM-2, 313 pM; NDM-1, 620 pM; L1, 637 pM) in standard assay mixture (50 mM HEPES pH 7.2, 50 µg/mL BSA, 0.01% Triton X-100) was incubated with inhibitor for 10 min at 30 °C then added to nitrocefin at concentrations resembling or identical to the K_M value for this substrate (IMP-1, 3.5 µM; VIM-2, 15 µM; NDM-1 1.0 µM; L1, 5.0 µM). Same day triplicates of assays performed in 96-well flat bottomed microplates (Corning, NY) were read at 482 nm for 5 min at 30 °C using a Spectramax 190 reader (Molecular Devices, Sunnyvale, CA).

Measurements for each compound were performed on 3 - 4 different days unless otherwise indicated. IC$_{50}$ values were obtained by fitting the equation below (Eq 1) to the recorded initial velocities using non-linear least squares regression.

Eq. 1:
$$y = \frac{100}{1+10^{(logIC50-[I])*s}}$$

Where *y* is the measured initial rate, [I] is the inhibitor concentration and *s* is the Hill slope.

K$_i$ Determination: Enzyme (60 pM IMP-1, 39.2 pM VIM-2, 600 pM NDM-1, 308 pM L1) was added to nitrocefin in excess of enzyme (25 µM for IMP-1, 100 µM for VIM-2, 15 µM for NDM-1, 50 µM for L1) containing various dilutions of inhibitor from the range of variable rates as determined from IC$_{50}$ experiments. The assay was performed in 50 mM HEPES pH 7.2 supplemented with 50 µg/mL BSA and 0.01% Triton X-100 in 96-well flat-bottomed

microplates to a final volume of 200 μL. All assays were read at 482nm using a SpectraMax 190 plate reader at 30 °C for 10 min. Progress curves were fitted by non-linear regression to Eq. 2:[54, 55]

$$[P]_t = v_s t + \frac{(v_0 - v_s)(1 - e^{-k_{obs}t})}{k_{obs}} + C$$

where $[P]_t$ is the product concentration at time t, v_0 and v_s are the initial and steady-state velocities, respectively, k_{obs} is the apparent first-order rate constant for the development of the steady state and the term C is included to correct for deviations of the baseline. Values of k_{obs} obtained at multiple concentrations of inhibitor [I] were then plotted against [I] and the result fitted to a straight line defined by Eq. 3:

$$k_{obs} = k_{-0} \left(1 + \frac{[I]}{K_i^{app}} \right)$$

where k_{-0} is the dissociation rate constant for the enzyme:inhibitor complex EI and K_i^{app} the apparent inhibition constant. Finally, K_i^{app} was used to determine K_i using Eq. 4:

$$K_i^{app} = K_i \left(1 + \frac{[S]}{K_M} \right)$$

Crystallization and structure determination.

IMP-1 and L1 were crystallized as previously described.[18, 51] Inhibitor-bound structures were obtained by soaking crystals in compound (2.5 mM) plus cryoprotectant (reservoir solution plus 25% glycerol) for 5 min (IMP-1 with **3a**) or 15 minutes (L1 with **3a** and **3b**). Crystals were subsequently flash-frozen in liquid nitrogen for data collection. Longer soaks for IMP-1 crystals resulted in severe deterioration of the crystal, while shorter soaks for L1 resulted in active sites which did not contain difference density suggestive of ligand binding. Datasets were collected at 100 K on beamline I02 (Diamond Light Source, UK), integrated in XDS[56] and scaled and merged using Aimless.[57] Phases were calculated by molecular replacement in Phaser[58] using PDB 1SML[51] and 5EV6[18] as search models for L1 and IMP-1, respectively. Structures were completed by iterative rounds of manual model building in Coot[59] and refinement in Phenix.[60] Ligand structures and geometric restraints were calculated with Phenix eLBOW. Structure validation was assisted by Molprobity[61] and Phenix. Figures were prepared using PyMol (www.pymol.org).

1
2
3
4
5
6
7
8
9
10
11
12
13
14
15
16
17
18
19
20
21
22
23
24
25
26
27
28
29
30
31
32
33
34
35
36
37
38
39
40
41
42
43
44
45
46
47
48
49
50
51
52
53
54
55
56
57
58
59
60

Protein structure accession numbers. Coordinates and structure factors have been deposited in the Protein Data Bank (PDB) under the following accession codes: IMP-1:**3a**, 5HH4; L1:**3a**, 5HH5; L1:**3b**, 5HH6.

Results and Discussion

PMPCs are *in vitro* inhibitors of B1 and B3 MBLs

Numerous classes of chelating agents, including 2-picolinic acid (**1**, **Figure 1**) and its derivatives, have been evaluated as potential MBL inhibitors.[13] In particular, dicarboxylate derivatives of pyridine have been reported to exhibit significant inhibitory activity against some MBLs.[30] These include dipicolinic acid (DPA, 2,6-pyridine dicarboxylate), which can inhibit the class B1 MBLs CcrA and IMP-1, and the B3 MBL L1[30, 62]; and 2,4-pyridine dicarboxylate, which inhibits the B2 MBL CphA.[30] However, DPA is a zinc chelator,[30] and has been shown to remove one zinc ion slowly from the active site of IMP-1 at high concentrations.[63] Further, a DPA derivative has been shown to be a sub-micromolar inhibitor of the B1 enzyme NDM-1.[64] Although the exact binding mode is not known, this compound did not strip NDM-1 of its metal ions, but bound to the active site. We have previously synthesized phosphonate-based derivatives of **1** (6-phosphonomethylpyridine-2-carboxylates, PMPCs) and showed them to be weak inhibitors (IC$_{50}$ 60-130 μM) of bacterial fructose-1,6-bisphosphate aldolase, an enzyme which uses a single zinc ion in its active site.[42] Here we test a selection of these derivatives, alongside some newly synthesized molecules (**Figure 1**), as potential inhibitors of the clinically relevant class B1 MBLs VIM-2, NDM-1 and IMP-1 and the class B3 MBL L1 (**Table 1**). We also tested **1** and 6-methyl-2-picolinic acid (**2; 1** with a methyl group at C6 of the pyridine ring), with both having a weak inhibitory effect towards the MBLs tested (IC$_{50}$ 32.2 μM to >100 μM), indicating that a single Zn-coordinating group on the pyridine ring cannot efficiently inhibit MBLs. The addition of a phosphonomethyl group on C6 of **1** (**3a**, PMPC-1) results in significant potency against all MBLs tested (IC$_{50}$ 0.374 – 3.88 μM) with a sub-micromolar IC$_{50}$ against the B1 MBL NDM-1. The addition of a hydroxyl group on the carbon of the phosphonomethyl group (**3b**, PMPC-2) had little effect compared to **3a** as IC$_{50}$ values were similar towards all MBLs tested. **3c** (PMPC-3) was synthesized with an additional large hydrophobic substituent on the phosphonomethyl group, with the aim of exploiting conserved hydrophobic areas within the active sites of B1 MBLs, particularly the flexible loop L3 (residues 60 – 66) previously implicated in substrate/inhibitor interactions.[65] Compared to **3a, 3c** exhibits slightly improved potency of about 1.2 – 2.8-fold against NDM-1, VIM-2 and IMP-1 (IC$_{50}$ 0.306 – 2.91 μM) and similar potency against L1 (~0.9-fold). The carboxylate on the 2-position of the pyridine ring, however, is essential as removal of this group (**4**) essentially abolishes MBL inhibitory activity of the PMPCs. The PMPC phosphonate compounds **3a**, **3b** and **3c** are therefore all low micromolar inhibitors of both B1 and B3 MBLs.

Identification of phosphonates as effective MBL inhibitors motivated more detailed kinetic studies aimed at probing the mode of inhibition for the PMPCs. Notably, nitrocefin hydrolysis progress curves, obtained without pre-mixing of enzyme and inhibitor, for both B1 (IMP-1, NDM-1, VIM-2) and B3 (L1) MBLs (**Figure 2** and **Figs. S1 - S3**) showed burst kinetics. This is consistent with observations that reliable IC_{50} values could only be obtained when enzyme and inhibitor were subjected to a 10 min pre-incubation before addition of substrate. These data strongly indicate that phosphonate inhibition of MBLs does not follow a simple competitive model, but that activity instead involves a time-dependent component. This behavior was apparent in the progress curves for inhibition by compounds **3a** (**Figure 2 and Fig. S1**), **3b** (**Fig. S2**) and **3c** (**Fig. S3**); in all cases these could be fitted using equation 2 as detailed in Methods.

Time-dependent or slow-binding inhibition[66] can be described by two alternative mechanisms (**Scheme 1**). In the simpler case, the inhibitory EI complex forms in a single, slow step, whereas in the more general case the initial inhibitory complex EI isomerizes slowly to form the steady-state enzyme-inhibitor complex EI*. These two models are distinguishable by replots of the derived first order rate constant k_{obs} against inhibitor concentration [I]; in the single step case k_{obs} increases linearly with [I]; in the two-step model dependence is instead hyperbolic. In all cases these secondary plots show linear dependence of k_{obs} on [I], leading us to conclude that formation of the inhibitory PMPC:MBL complex occurs in a single step.
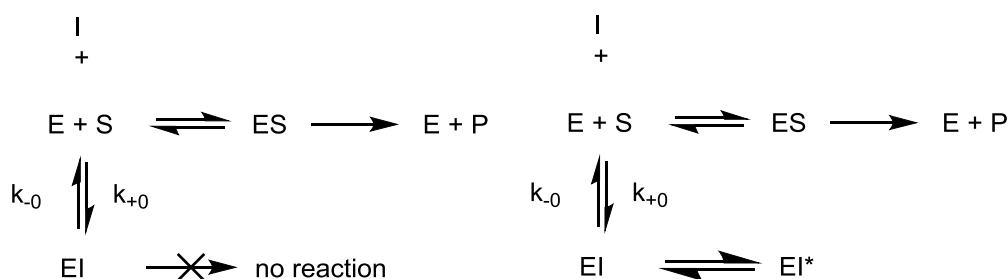
Scheme 1: Possible Mechanisms for Slow-binding Inhibition. In the simpler case (left; observed here), the inhibitory complex EI forms by a single, slow step. In the more general case (right) the initial inhibitory complex EI isomerizes slowly to form the steady-state inhibitory complex EI*.
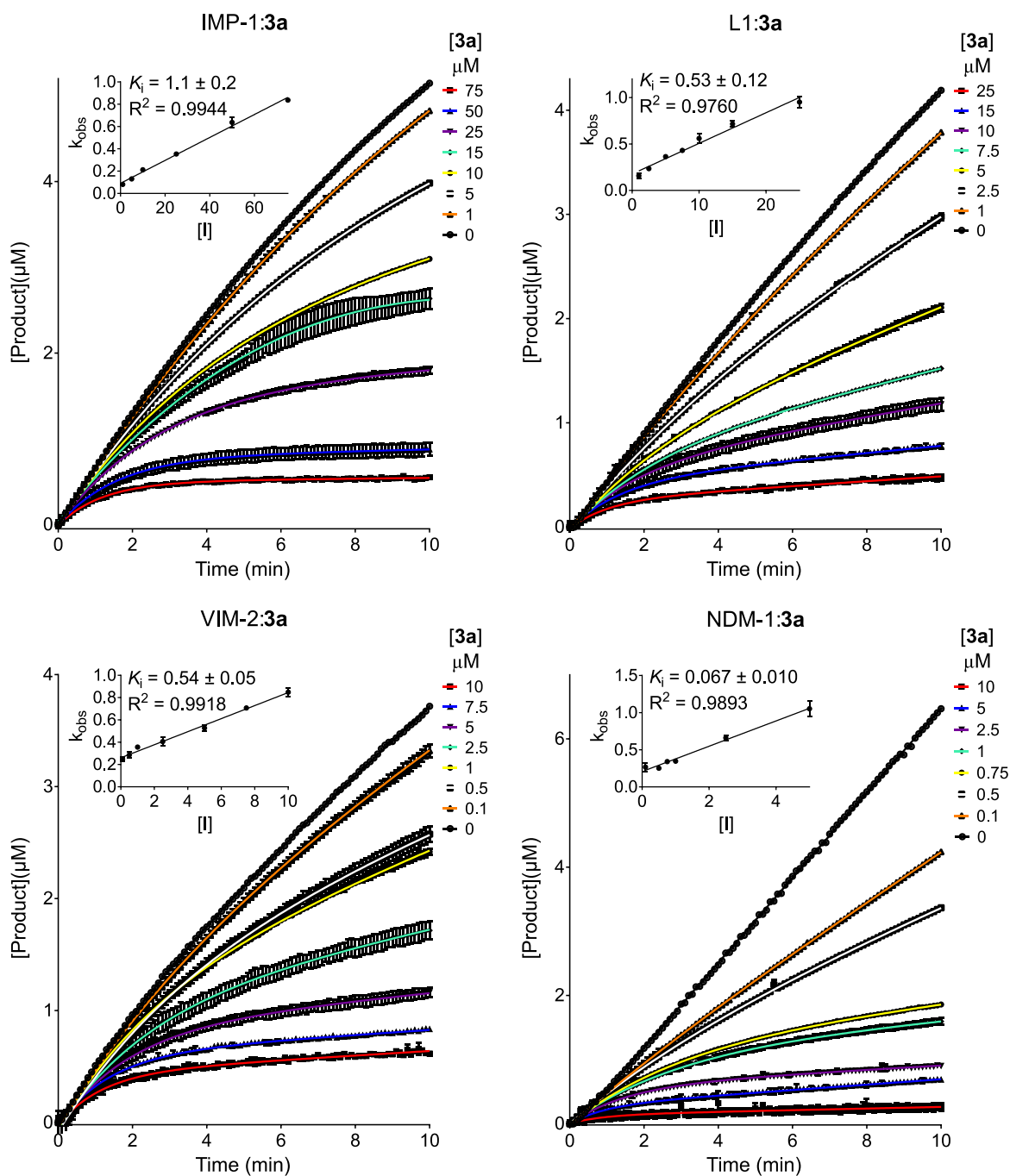
12

1
2
3
4
5
6
7
8
9
10
11
12
13
14
15
16
17
18
19
20
21
22
23
24
25
26
27
28
29
30
31
32
33
34
35
36
37
38
39
40
41
42
43
44
45
46
47
48
49
50
51
52
53
54
55
56
57
58
59
60

Figure 2. 3a Inhibits MBLs by a Time-Dependent Mechanism. Progress curves and secondary linear plots (insets) for **3a** inhibition of nitrocefin hydrolysis by IMP-1, L1, NDM-1 and VIM-2. Curve fitting procedure is described in the text. The error bars in the progress curves represent three technical replicates.

13

Using this treatment, we determined inhibition constants (K_i) for the phosphonates **3a**, **3b** and **3c** against VIM-2, NDM-1, IMP-1 and L1. As with the IC_{50} data, K_i values (**Table 2**) indicate the compounds to be similarly potent, showing particularly dramatic effect against NDM-1 (K_i 34 – 74 nM). As described above, **3a**, **3b** and **3c** all demonstrated a slow-binding competitive inhibition profile against all MBLs, with a slow "on" rate and even slower "off" rate (**Table S1**) but no isomerization step. Inspection of the rate constants in Table S1 shows a range of values for the on rate (k_0) between 0.08 and 6.4 s^{-1}, i.e. almost two orders of magnitude, whilst the off rate (k_{-0}) exhibits less variation. Of the four enzymes tested, values for k_0 are consistently highest for NDM-1, and consistently lowest for IMP-1, which also exhibits the lowest k_{-0} values. Comparison of values for the different compounds reveals that PMPC **3c**, which incorporates relatively hydrophobic functionalities, has higher on rate constants (k_0) for the B1 MBLs (IMP-1, NDM-1 and VIM-2) than do the other PMPCs, although no difference is observed for the B3 L1 enzyme.

Previous descriptions of slow-binding inhibition of MBLs, e.g. of IMP-1 by certain thiols,[67] or of the model MBL *Bacillus cereus* BcII by thiols formed on opening of the dihydrothiazine ring of cephalosporins,[68] propose that slow-binding is likely due to involvement of an isomerization step in formation of the inhibitory complex EI* (**Scheme 1**). An alternative explanation is necessary to account for the single-step pathway observed here. In this context we note recent molecular dynamics simulations[69] suggesting that slow-binding may arise, at least for some inhibitors, because of favorable interactions of the inhibitor with transient enzyme-bound water molecules present on initial association and that are removed by step-wise dehydration to generate the final inhibitory complex. It is reasonable to suggest that such mechanisms may be involved in the slow-binding inhibition of MBLs by PMPCs, particularly given the polar character of these compounds. This could also explain why, unlike the case for B1 MBLs tested, the on rate (k_0) for PMPC **3c** inhibition of L1 does not differ substantially from those observed for **3a** and **3b**. One consequence of the structural differences between the B1 and B3 enzymes may be differing spatial distributions of water molecules within and near the active sites, requiring a different pathway to be taken from the initial, hydrated, complex to the stable, inhibitory complex analogous to that formed with the B1 enzymes.

The off-rate constants (k_{-0}) in **Table S1** also provide some insight in to the residency times of PMPC inhibitors at the MBL binding sites, which may be calculated as dissociative half-lives ($t_{1/2} = 2 / k_{-0}$) and are summarized in **Table S2**. Values range from 6 (complex of **3b** and VIM-2) to 25 (**3c**:IMP-1) minutes. Recent work[70-73] highlights the importance of assessing kinetic

data on drug-target residence time, as well as equilibrium binding constants, in analyzing structure-activity relationship data during lead optimization of drug candidates. Long residency time can extend the duration of drug effects *in vivo* and enhance selectivity if the residency time exceeds those for related off-target enzymes. Such considerations will play an important role in our future efforts to advance the PMPCS towards compounds with clinical potential.

In addition to the distinctive slow-binding behavior observed here, the kinetics observed with the PMPCs also differ from those observed for the natural product aspergillomarasmine A that attenuates NDM-1 and VIM-2 activity (but not that of IMP-7 or the B3 enzyme AIM) by removing both zinc ions.[44] Notably, these compounds are more potent against a greater range of MBL targets than captopril,[14] and show similar, and sometimes better, potency than other thiol-based compounds such as mercaptophosphonates,[27] with IC_{50} values ranging from 0.3-7.2 µM across all MBL/inhibitor combinations tested.

PMPCs enhance meropenem antibacterial activity against MBL-producing bacteria

We next tested the ability of the simplest of our synthesized phosphonate compounds, **3a**, to enhance the antibacterial activity of meropenem against bacterial strains producing the most clinically relevant subclass B1 MBLs from introduced broad-host range plasmids or clinical isolates. Meropenem MIC was first measured using bacteria expressing the cloned MBLs IMP-1 (*E. coli*), VIM-1 (the most prevalent VIM MBL subtype in Enterobactaeriaceae[74], (90.6% sequence identity to VIM-2), *E. coli*) and NDM-1 (*E. coli*, *K. pneumoniae*, *C. freundii* and *E. aerogenes*) (**Table 3**). In all cases, other than that of VIM-1, expression in the laboratory *E. coli* strain MG1655, MBL expression conferred resistance to meropenem as adjudged by CLSI (resistance is defined by MIC $\geq$ 4 mg/L for Enterobacteriacae and $\geq$ 8 mg/L for *P. aeruginosa*) or EUCAST (resistance MIC >8 mg/L for Enterobacteriacae and *P. aeruginosa*) breakpoints.[48, 75] Co-administration with **3a** reduced meropenem MICs into the susceptible range against all strains except *E. coli* MG1655 expressing NDM-1 (MIC 8 mg/L), although this required 100 mg/L **3a** to achieve. In all cases, at 100 mg/L **3a**, the meropenem MIC was reduced by at least 16-fold. Against *K. pneumoniae*, *C. freundii* and *E. aerogenes* expressing NDM-1, MICs were enhanced to 4, 2 and 1 mg/L, respectively, but not restored to meropenem MICs against non MBL-producing strains ($\leq$0.25[33], 0.06 and 0.06 mg/L[76]). For wild-type clinical isolates (*Pseudomonas putida*, *P. aeruginosa*, *S. maltophilia,* one *K. pneumoniae* and one *E. coli*) (**Table 4**), a similar trend was observed, with some reduction in meropenem MIC against all 9

15

strains tested. There was a greater than 4-fold reduction of meropenem MIC against eight out of the nine strains tested at 128 mg/L **3a**, with five out of nine strains reverting from meropenem resistance to susceptibility (EUCAST definition meropenem MIC ≤ 2 mg/L) at the same concentration of **3a**. In the case of the NDM-1-producing *K. pneumoniae* clinical isolate in **Table 4**, a meaningful comparison of the potency of **3a** and AMA is possible since this same strain has been employed in a study on the effect of AMA on meropenem MIC.[44] The MIC for meropenem was reduced to 0.25 mg/L in the presence of 16 mg/L AMA, and to <0.125 mg/L in the presence of 32 mg/L. Here, the MIC for meropenem was found to be reduced to 0.25 mg/L in the presence of **3a** at 32 mg/L and to <0.125 mg/L at 64 mg/L of the inhibitor. Notably, **3a** enhanced meropenem activity against an *E. coli* strain (UWB75) carrying both an SBL (CTX-M-15, which lacks meaningful carbapenemase activity) and the NDM-1 MBL (4-fold reduction at 32 mg/L inhibitor; greater than 512-fold reduction, from 128 to < 0.25 mg/L, at 128 mg/L).

Compounds **3b** and **3c** were next tested against a subset of clinical MBL-producing strains in a preliminary assessment of the effects of substitutions upon biological activity (**Table S3**). Importantly, in all cases we observed reductions in meropenem MICs in the presence of PMPCs, although the effects were variable. The modifications in **3b** and **3c** exerted a similar effect compared to **3a** upon the potency of meropenem combinations against *E. coli* UWB93 and *K. pneumoniae* UWB116. However, against *E. coli* UWB75 (the isolate for which meropenem MIC was highest) the effectiveness of both **3b** and **3c** was reduced, with **3c** unable to restore meropenem susceptibility at 128 mg/L. **3b** and **3c** were also less effective against the two *Pseudomonas* spp. strains for which, unlike **3a**, neither compound could restore meropenem susceptibility, even at 128 mg/L. Despite the difference in size, **3b** and **3c** behaved identically towards the *P. putida* isolate UWB24, whereas for *P. aeruginosa* UWB78 **3c** appeared less effective than **3b**, although the effects were subtle (4-fold difference in meropenem MIC at the highest concentration tested). These data indicate that modifications to the PMPC scaffold affect, but do not abolish, activity in bacterial growth assays. Indeed, the potency against Enterobacteriaceae (a group of pathogens in which MBL-mediated carbapenem resistance is particularly concerning) was in many cases tolerant of additions to the PMPCs.

We also tested activity of **3a** against *S. maltophilia*, a notoriously impermeable pathogen of compromised individuals and a growing problem in cystic fibrosis patients.[77, 78] Compared to

16

the *E. coli, K. pneumoniae* and *Pseudomonas* spp. isolates, activity of **3a**, was reduced (**Table 4**). Nevertheless, **3a** was able to potentiate meropenem activity (4-fold reduction in MIC values) against the clinical multi-drug resistant *S. maltophilia* bloodstream isolate K279a. To determine whether PMPC potency is influenced by efflux, we measured MICs in a K279a derivative overexpressing the resistance nodulation division (RND) efflux pump SmeYZ (*S. maltophilia* K ami32), and an additional knock-out strain lacking the RND pumps SmeJ/K/W/Z/P (*S. maltophilia* JKWZP). In the presence of **3a**, meropenem MICs were reduced by a single 2-fold dilution against the overexpression strain K ami32, and 4-fold against the JKWZP efflux pump knockout strain, suggesting that PMPCs are only slightly affected by efflux in *S. maltophilia*.

Taken together, these experiments indicate that PMPCs, in particular **3a**, are able to inhibit a range of MBLs expressed in the periplasm and enhance β-lactam activity against a wide range of Gram-negative bacteria. While relatively high PMPC concentrations (32 to 128 mg/L) were required to restore meropenem susceptibility (which was not always achieved), activity was observed against a range of target species, including non-fermenters, and was relatively unaffected by alterations to known efflux systems. These data indicate that, while compounds in this initial series may not show optimal penetration of the Gram-negative outer membrane, some entry into the periplasm is occurring even in problematic species such as *P. aeruginosa* and *S. maltophilia*. This supports our contention that these initial examples of the PMPC scaffold can be viable lead structures for further optimization. Importantly, we consider this to remain valid despite the presence of multiple ionizable groups which might be expected to create complications with respect to pharmacokinetics or drug delivery. The literature pK_a values of approximately 2.5 and 8 respectively, for the first and second ionizations of phosphonates,[79] and of 1.0 for 2-picolinic acid[80] lead us to expect that at physiological pH the PMPCs will exist largely in a di-anionic form. Given the ample precedents for dianionic β-lactams (e.g. carbenicillin or ticarcillin[81]) being suitable for clinical use as antibiotics for Gram-negative bacteria, including *Pseudomonas aeruginosa*, we do not expect the ionization state of these inhibitors to be necessarily problematic.

Although a previous study showed **3a** to be non-toxic to immortal African green monkey kidney cells (BL-C-1),[82] due to the relatively high concentrations (up to 100 mg/L) of inhibitor required for significant reduction in MIC, we tested the toxicity of **3a** against Caco-2 (human epithelial), HEPG2 (human liver) and H4IIE (rat hepatoma) cells at higher concentrations. These data show **3a** does not affect the metabolic activity, membrane integrity or lysosome

17

integrity of these cell lines until concentrations significantly higher than those at which MIC reductions are observed, with EC_{50} values 242 mg/L and greater (**Table S4**).

Structure determination of MBLs complexed with phosphonate compounds

To understand the mechanism of MBL inhibition by PMPCs, we have obtained crystal structures of the B1 MBL IMP-1 (an enzyme found on plasmids in a range of Gram-negative bacterial pathogens, particularly *P. aeruginosa*) in complex with **3a** (2.0 Å resolution) and the B3 L1 enzyme (encoded on the chromosome of *S. maltophilia*) in complex with both **3a** (1.80 Å) and **3b** (1.80 Å) (**Table S5**). IMP-1 crystallized in the space group $P2_12_12_1$ with four molecules in the asymmetric unit (ASU), as previously described (PDB 5EV6[18]). **3a** could be modelled into well-defined difference electron density (**Figure 3A**) in two out of the four chains in the ASU, with full occupancies and B-factors 1.3 times above the protein main chain (chain A validation statistics, RSCC 0.96, RSR 0.12 and LLDF 1.95). L1 crystallized in the space group $P6_422$, as previously described,[51] with one molecule in the ASU. Difference electron density consistent with **3a** or **3b** (**Figure 3B and 3C**, respectively) was observed in the active sites of the two crystal structures and ligands were refined at full or 0.84 occupancy to B-factors 1.9 and 1.7 times above protein main chain, respectively (RSCC 0.96/0.93, RSR 0.16/0.14 and LLDF 3.94/5.64).
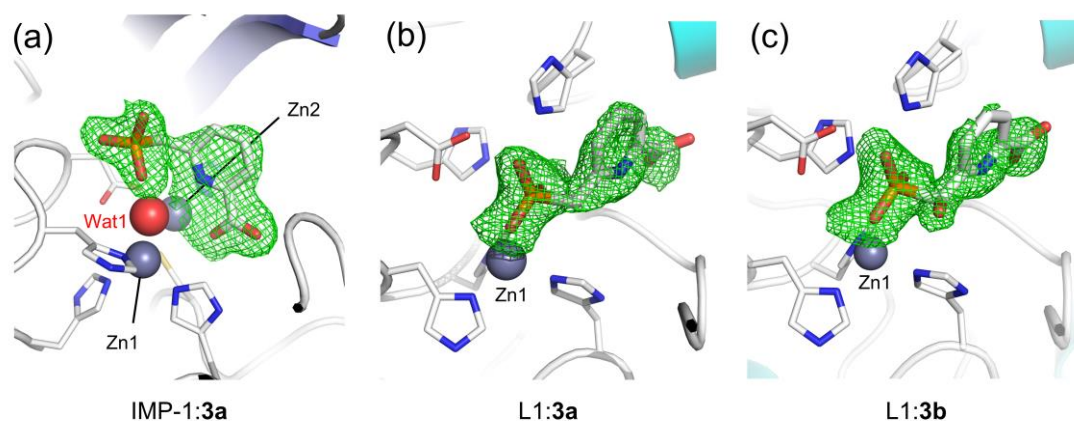
Figure 3. Binding of PMPC Inhibitors to MBL active sites.

Close up of the active sites of MBL:PMPC complexes. Zinc ions and the nucleophilic water/hydroxide (gray and red spheres, respectively) are labelled. Zinc ligands are shown as sticks. F_o-F_c density (green, contoured at 3σ) is calculated from the final model with the ligand (sticks) omitted. **(a)** B1 IMP-1 complexed with **3a**. **(b)** B3 L1 complexed with **3a**. **(c)** B3 L1 complexed with **3b**.

1
2
3
4
5
6
7
8
9
10
11
12
13
14
15
16
17
18
19
20
21
22
23
24
25
26
27
28
29
30
31
32
33
34
35
36
37
38
39
40
41
42
43
44
45
46
47
48
49
50
51
52
53
54
55
56
57
58
59
60

Mode of PMPC binding to the B1 MBL IMP-1 di-zinc center.

3a binds to the di-zinc active site of IMP-1 but does not displace the nucleophilic hydroxide (Wat1, **Figure 4A**). **3a** adopts the same conformation in chains A and B, interacting with the Zn2 ion, nucleophilic hydroxide and residues on the protein main chain (**Figure 4A**), but binding does not result in global changes in conformation in comparison to the uncomplexed enzyme structure (PDB 5EV6,[18] RMSD=0.21 Å, chain A, over 218 Cα residues). The inhibitor carboxylate group and pyridine nitrogen atom both interact with the Zn2 site, at distances of 2.30 Å and 2.69 Å (chain A measurements throughout, unless otherwise stated; see **Fig. S4** for a schematic comparison of binding in chains A and B), respectively, resulting in a zinc ion with six ligands in a distorted octahedral geometry, in contrast to Zn2 in uncomplexed IMP-1 which has a distorted trigonal bipyramidal geometry. The carboxylate also interacts with Lys224 on the protein main chain (2.70 Å), and binding is further stabilized by the close proximity of a hydrophobic pocket (Val61, Val67, Trp64, Phe87, **Fig. S5**). A weak T-shaped interaction[83] of the pyridine ring with the face of the indole ring of Trp64 on the flexible loop L3 (pyridine C4 to indole C3 distance 3.72 and 3.94 Å in chains A and B respectively) is also observed. The pyridine nitrogen is also positioned close to the zinc-bridging hydroxide (Wat1 in **Figures 3-5**; 2.9 Å), with the torsion about the phosphonate C-P bond approximately 90° relative to the plane of the pyridine ring. Surprisingly, the phosphonate makes limited interactions with the active site, and is too distant from the zinc ions for productive interactions (the closest O atom is 3.89 Å from Zn1 and 4.35 Å from Zn2), instead forming hydrogen bonds with the bridging water/hydroxide (Wat1) (2.58 Å) and the side chain of Ser119 (3.26 Å).
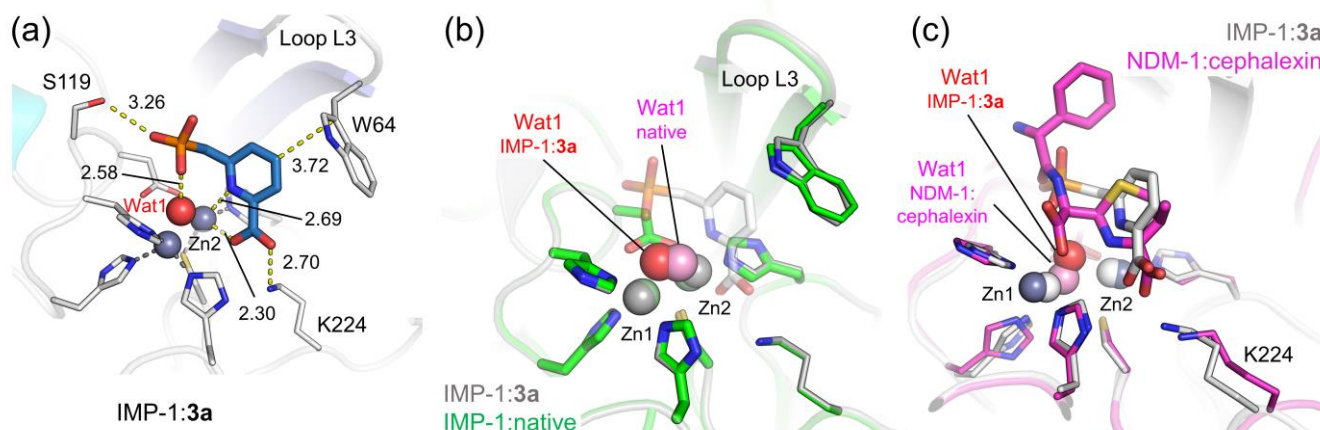
19

Figure 4. Binding mode of 3a to B1 MBL IMP-1

PMPC and antibiotic are shown as sticks. Zn sites and nucleophilic waters/hydroxides (Wat1) are labelled. **(a) 3a** (blue sticks) bound to the active site of IMP-1. Ligand interactions (distances labelled) and zinc-protein interactions are shown as yellow and gray dotted lines, respectively. **(b)** Superposition of the IMP-1:**3a** complex (gray) with uncomplexed IMP-1 (green, PDB 5EV6). **(c)** Superposition of the IMP-1:**3a** complex (gray) with the NDM-1:hydrolysed cephalexin complex (pink, PDB 5EV6). IMP-1 zinc ions are light grey and NDM-1 zinc ions dark grey.

As well as making interactions with the bridging hydroxide, the **3a**:IMP-1 complex contains an additional water molecule associated with the inhibitor. This water molecule (blue WatA in **Fig. S4** and **Fig. S6**; B-factor 34 Å^2) is located on the same face of the pyridine ring as the phosphonate group and is within H-bonding distance (2.63 Å) to the phosphonate oxygen atom that interacts with the bridging hydroxide. Furthermore, this WatA contacts the π-bond between N and C2 of the pyridine ring (3.03 and 3.17 Å to the pyridine N and C2 atoms, respectively). This attraction may arise from the somewhat electron deficient nature of this π-bond resulting from interaction of the pyridine nitrogen with Zn2. WatA is also within H-bonding distance of the bridging hydroxide (2.84 Å) and relatively close to Zn1 (3.21 Å) as well as to two of its ligands, His118 and His196 (see **Fig. S4**). The presence of, and relatively extensive interactions made by WatA lead us to speculate that the IMP-1-bound inhibitory species is the hydrated form of **3a**. This may explain why PMPC inhibition does not involve displacement of the bridging hydroxide (see below) as the associated loss of WatA would be expected to be energetically unfavorable.

In chains C and D, where electron density for bound PMPC could not be resolved, the active site zinc ions were refined with lower occupancies (^{C}Zn1, 0.94; ^{C}Zn2, 0.87; ^{D}Zn1, 0.51; ^{D}Zn2, 1.0), suggesting that exposure to **3a** may have depleted zinc content. This may be a reason for the lack of observable inhibitor electron density in these active sites. The potential for a carboxylate-containing pyridine to remove zinc from the IMP-1 active site has been noted previously, as incubation of IMP-1 with DPA resulted in Cys221 (Zn2 ligand) becoming more accessible to chemical modification.[84]

In comparison with uncomplexed IMP-1, there is little change in either protein side chain or zinc positions (**Figure 4B**). In particular, the flexible loop L3 and the π -stacking Trp64 are in the same conformation, most likely due to crystal contacts in the ASU.[18] Interactions of loop L3 residues with bound inhibitors frequently feature in inhibitor complexes of B1 MBLs.[16, 21, 65, 85] The Zn1 – Zn2 separation is similar (3.54 Å in IMP-1:**3a**; 3.42 Å in uncomplexed IMP-1), although there is a slight (0.5 Å) shift in the position of Zn2 which in the inhibitor complex increases the distances to the Asp120 (1.98 Å uncomplexed, 2.16 Å **3a**-bound) and Cys221 (2.31 Å uncomplexed, 2.42 Å **3a**-bound) ligands. There is a more significant (*c*. 1 Å) movement of the bridging nucleophilic water/hydroxide compared to uncomplexed IMP-1). This causes the water to be near equidistant between Zn1 and Zn2 (2.05 Å and 2.21 Å, respectively), whereas in the uncomplexed enzyme the nucleophilic water/hydroxide is 1.87 Å and 2.43 Å away from Zn1 and Zn2, respectively. Interaction of an MBL inhibitor with the nucleophilic hydroxide is unusual, and to our knowledge has only been observed once before, in the interaction of the *Bacteriodes fragilis* B1 MBL CfiA with a tricyclic carboxylate.[86] Far more common are inhibitor binding modes that involve displacement of the bridging hydroxide.

Interactions made by **3a** also share some aspects of antibiotic binding to B1 MBLs. As to date there is no crystal structure available of IMP-1 bound to either intact or hydrolyzed antibiotic, in **Figure 4C** we show a superposition of IMP-1:**3a** with NDM-1 complexed with the hydrolyzed cephalosporin cephalexin (chain B of PDB 4RL2[20]). As in inhibitor binding, the carboxylate of the cephalosporin dihydrothiazine ring interacts with both Zn2 and Lys224, while the β-lactam nitrogen also contacts Zn2 forming a distorted (though face monocapped) octahedral geometry. Thus **3a** binding replicates some aspects of interactions of B1 MBLs with their β-lactam substrates. However, the two complexes differ substantially in that the interactions involving the carboxylate group of hydrolyzed antibiotic create a trigonal

21

bypyrimidal geometry about Zn1, in contrast to the regular tetrahedral geometry of Zn1 observed in the IMP-1:**3a** complex.

PMPC binding to B3 L1 defines a structurally distinct mode of inhibition

Crystal structures of complexes of the B3 MBL L1 with **3a** and **3b** reveal an unprecedented mode of inhibitor binding (**Figures 5A and 5B**). Surprisingly, despite our *in vitro* kinetic data (above) indicating a similar mode of inhibition of both IMP-1 and L1, the phosphonate moiety of both compounds replaces the zinc ion in the Zn2 site of L1, forming a monozinc enzyme in which only the Zn1 site is occupied. The PMPC therefore does not strip the L1 active site of both zinc ions, even at such high inhibitor concentrations, indicating that the PMPC binds specifically to the MBL active site. Removal of zinc from the Zn2 site has only previously been seen by incubation of L1 with relatively high concentrations (10 mM) of EDTA.[26] In the present case, zinc displacement by **3a** results in tight interaction of the phosphonate directly with components of the di-zinc center of the MBL. In particular, in both the **3a** and **3b** complexes there is a strong interaction (1.80 Å) of the phosphonate group with Zn1 (**Fig. S7**). This is notably tighter than the contacts with the three Zn1 His- ligands (~2.1 Å). The phosphonate also makes multiple interactions with the amino acid side chains that normally constitute the Zn2 site in L1 - His121 (2.89/2.68 Å, **3a**/**3b**), Asp120 (2.35/2.34 Å), His263 (2.68/2.56 Å). Comparison of the **3a** and **3b** structures shows the hydroxyl group of the **3b** phosphonate to be uninvolved in binding, although, notably, the high quality of the observed electron density makes it clear that a single enantiomeric form of the inhibitor (the S- rather than R- isomer) is selectively bound to the L1 active site, although the compound was synthesized as a racemic mixture.
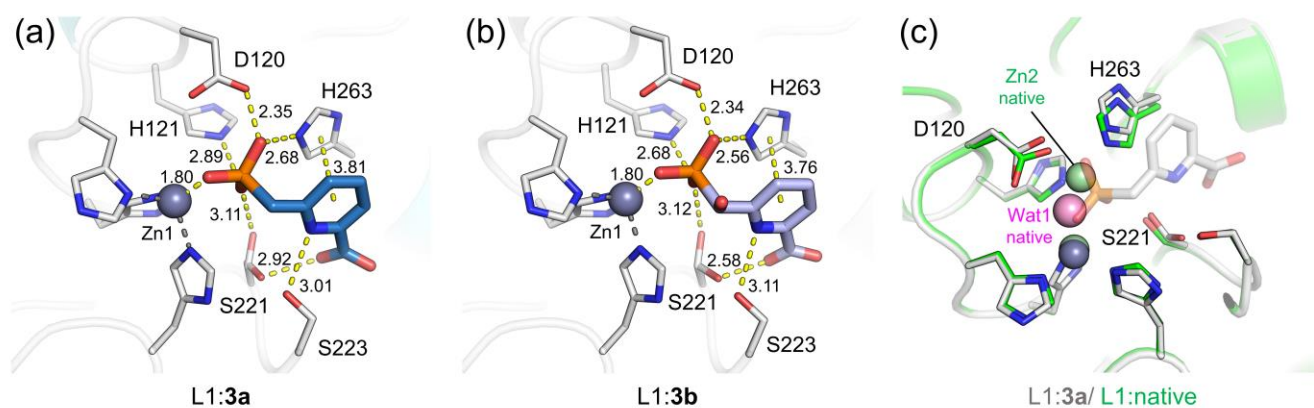
22

Figure 5. Binding mode of PMPCs to B3 MBL L1. Representations are as Figure 3. L1 interactions with **(a) 3a** and **(b) 3b**. **(c)** Superposition of the L1:**3a** complex (gray) with uncomplexed L1 (green).

In comparison to uncomplexed L1 (**Figure 5C** shows a superposition of L1:**3a**, gray, with uncomplexed L1, green, PDB 1SML) there is little change in overall structure (L1:**3a**/L1:**3b** Cα RMSD=0.233/0.234 Å over 266 residues). However, phosphonate binding to the Zn2 site causes not only removal of the zinc ion but also significant conformational changes within the active site. In particular, there are ~0.8 Å and ~0.6 Å movements of His263 and Asp120, respectively, away from the active site. One of the phosphonate oxygen atoms also replaces the nucleophilic water/hydroxide, which, in contrast, is retained on binding of the hydrolyzed β-lactam moxalactam.[51] Ser221 on the protein main chain, which stabilizes hydrolyzed substrate through interactions with the C3/C4 carboxylate group,[19] forms a dual conformation where it interacts either with the PMPC phosphonate (3.11/3.12 Å) or carboxylate (2.92/2.58 Å) groups. These two conformations could be refined with similar occupancies (0.64/0.36 on **3a** binding, and 0.49/0.51 on **3b** binding). Ser223, which also forms contacts with the carboxylate of hydrolyzed substrate, interacts here with the nitrogen of the pyridine ring (3.01/3.11 Å). These interactions suggest that, despite the very different mode of PMPC binding compared to that of hydrolyzed antibiotic,[19] the two serine residues on the protein main chain remain key to ligand stabilization within the active site.

Observation of different modes of PMPC binding in our crystal structures, i.e. monozinc L1 and dizinc IMP-1 complexes, was unexpected. However, the consistency between inhibition kinetics across the MBL systems investigated leads us to conclude that, at least under the conditions of our kinetic experiments, PMPCs are able to form an inhibitory complex with di-zinc L1 similar to that observed with IMP-1. In the crystallization experiments, where enzyme

and inhibitor concentrations are much greater, this may serve as a precursor to the observed more stable complex from which the zinc ion has been lost from the L1 Zn2 binding site. The fact that such a complex is not observed with IMP-1 may then reflect differences in the metal-binding properties of the two enzymes: whereas zinc binding to L1 is proposed to be sequential,[87] with the Zn1 site bring occupied first, zinc binding to IMP-1 is instead proposed to be positively cooperative.[88] As such selective removal of zinc from the Zn2 site, as observed in L1, would be disfavored in the IMP enzyme. Furthemore, we note favorable contacts made by PMPC inhibitors with L1 sidechain functionalities (e.g. the imidazole ring of His121 and the primary hydroxyl group of Ser221) that are not present in the actives site of the B1 enzymes such as IMP (Fig. S7), and that may additionally promote displacement of the Zn2 ion by PMPCs.

Conclusions

Phosphonate-based compounds have been an underexplored and poorly characterized area of MBL inhibitor design. Here we show they can inhibit a wide range of MBLs, both *in vitro* and in pathogenic Gram-negative bacteria, including non-fermenting organisms that are frequently difficult to penetrate with small molecule agents. Despite the potential for phosphonate compounds to act as zinc-chelators, we show crystallographically that they can bind specifically to the active site of MBLs, either through a conventional (i.e. replicating interactions of physiological substrates) mechanism of binding to the Zn2 site in an otherwise largely unperturbed active site (B1 IMP-1); or by the unprecedented mechanism of replacing Zn2 (B3 L1). Importantly, despite this ability to remove a zinc ion from the di-zinc active site of L1, they are non-toxic to human cell lines at concentrations significantly above levels required to potentiate antibiotic activity. Therefore, unlike promising compounds such as aspergillomarasmine A (AMA), PMPCs inhibit MBLs by binding to the active site, and not simply by chelating the metal ions.

The structural information presented here will also allow us to identify routes to rational modification of the PMPCs to enhance their affinity for the active sites of both B1 and B3 MBLs. In particular, the mode of binding to IMP-1 reveals potential attachment sites on the core PMPC structure (e.g. ortho to the carboxylate group) where functionalities known to

24

enhance the uptake of β-lactam antibiotics (e.g. siderophores[89]) might be introduced without interfering with the favourable interactions of the inhibitors with the MBL active site.

In summary, our data indicate that phosphonates, in particular 2-picolinic acid derivatives that combine submicromolar potency against multiple MBL targets with a simple scaffold amenable to further decoration, can be further considered and developed as lead compounds for novel MBL inhibitors.

Conflicts of Interest

There are no conflicts to declare.

Supporting Information

Supplemental Figures 1-7

Supplemental Tables 1-5

Synthetic Procedures (includes supplemental figures 8-29)

Acknowledgments

References

[1] Bush, K. (2013) Proliferation and significance of clinically relevant beta-lactamases, *Ann N Y Acad Sci 1277*, 84-90.

[2] Walsh, T. R. (2010) Emerging carbapenemases: a global perspective, *Int J Antimicrob Agents 36 Suppl 3*, S8-14.

[3] van Duin, D., Kaye, K. S., Neuner, E. A., and Bonomo, R. A. (2013) Carbapenem-resistant Enterobacteriaceae: a review of treatment and outcomes, *Diagn Microbiol Infect Dis 75*, 115-120.

[4] Karsisiotis, A. I., Damblon, C. F., and Roberts, G. C. (2014) A variety of roles for versatile zinc in metallo-beta-lactamases, *Metallomics 6*, 1181-1197.

[5] Fisher, J. F., Meroueh, S. O., and Mobashery, S. (2005) Bacterial resistance to beta-lactam antibiotics: compelling opportunism, compelling opportunity, *Chem Rev 105*, 395-424.

[6] Bush, K. (2010) Alarming beta-lactamase-mediated resistance in multidrug-resistant Enterobacteriaceae, *Curr Opin Microbiol 13*, 558-564.

[7] Palzkill, T. (2013) Metallo-beta-lactamase structure and function, *Ann N Y Acad Sci 1277*, 91-104.

[8] Galleni, M., Lamotte-Brasseur, J., Rossolini, G. M., Spencer, J., Dideberg, O., Frere, J. M., and Metallo-beta-lactamases Working, G. (2001) Standard numbering scheme for class B beta-lactamases, *Antimicrob Agents Chemother 45*, 660-663.

[9] Bebrone, C. (2007) Metallo-beta-lactamases (classification, activity, genetic organization, structure, zinc coordination) and their superfamily, *Biochem Pharmacol 74*, 1686-1701.

[10] Meini, M. R., Llarrull, L. I., and Vila, A. J. (2015) Overcoming differences: The catalytic mechanism of metallo-beta-lactamases, *FEBS Lett 589*, 3419-3432.

[11] Fonseca, F., Bromley, E. H., Saavedra, M. J., Correia, A., and Spencer, J. (2011) Crystal structure of Serratia fonticola Sfh-I: activation of the nucleophile in mono-zinc metallo-beta-lactamases, *J Mol Biol 411*, 951-959.

[12] Bush, K., and Jacoby, G. A. (2010) Updated functional classification of beta-lactamases, *Antimicrob Agents Chemother 54*, 969-976.

[13] Fast, W., and Sutton, L. D. (2013) Metallo-beta-lactamase: inhibitors and reporter substrates, *Biochim Biophys Acta 1834*, 1648-1659.

[14] Brem, J., van Berkel, S. S., Zollman, D., Lee, S. Y., Gileadi, O., McHugh, P. J., Walsh, T. R., McDonough, M. A., and Schofield, C. J. (2015) Structural Basis of Metallo-beta-Lactamase Inhibition by Captopril Stereoisomers, *Antimicrob Agents Chemother 60*, 142-150.

[15] Lienard, B. M., Garau, G., Horsfall, L., Karsisiotis, A. I., Damblon, C., Lassaux, P., Papamicael, C., Roberts, G. C., Galleni, M., Dideberg, O., Frere, J. M., and Schofield, C. J. (2008) Structural basis for the broad-spectrum inhibition of metallo-beta-lactamases by thiols, *Org Biomol Chem 6*, 2282-2294.

[16] González, M. M., Kosmopoulou, M., Mojica, M. F., Castillo, V., Hinchliffe, P., Pettinati, I., Brem, J., Schofield, C. J., Mahler, G., Bonomo, R. A., Llarrull, L. I., Spencer, J., and Vila, A. J. (2015) Bisthiazolidines: A Substrate-Mimicking Scaffold as an Inhibitor of the NDM-1 Carbapenemase, *ACS Infectious Diseases*.

[17] Mojica, M. F., Mahler, S. G., Bethel, C. R., Taracila, M. A., Kosmopoulou, M., Papp-Wallace, K. M., Llarrull, L. I., Wilson, B. M., Marshall, S. H., Wallace, C. J., Villegas, M. V., Harris, M. E., Vila, A. J., Spencer, J., and Bonomo, R. A. (2015) Exploring the Role of Residue 228 in Substrate and Inhibitor Recognition by VIM Metallo-beta-lactamases, *Biochemistry 54*, 3183-3196.

[18] Hinchliffe, P., Gonzalez, M. M., Mojica, M. F., Gonzalez, J. M., Castillo, V., Saiz, C., Kosmopoulou, M., Tooke, C. L., Llarrull, L. I., Mahler, G., Bonomo, R. A., Vila, A. J., and Spencer, J. (2016) Cross-class metallo-beta-lactamase inhibition by bisthiazolidines reveals multiple binding modes, *Proc Natl Acad Sci U S A 113*, E3745-3754.

26

[19] Spencer, J., Read, J., Sessions, R. B., Howell, S., Blackburn, G. M., and Gamblin, S. J. (2005) Antibiotic Recognition by Binuclear Metallo-β-Lactamases Revealed by X-ray Crystallography, *Journal of the American Chemical Society 127*, 14439-14444.

[20] Feng, H., Ding, J., Zhu, D., Liu, X., Xu, X., Zhang, Y., Zang, S., Wang, D. C., and Liu, W. (2014) Structural and mechanistic insights into NDM-1 catalyzed hydrolysis of cephalosporins, *J Am Chem Soc 136*, 14694-14697.

[21] Brem, J., van Berkel, S. S., Aik, W., Rydzik, A. M., Avison, M. B., Pettinati, I., Umland, K. D., Kawamura, A., Spencer, J., Claridge, T. D., McDonough, M. A., and Schofield, C. J. (2014) Rhodanine hydrolysis leads to potent thioenolate mediated metallo-beta-lactamase inhibition, *Nat Chem 6*, 1084-1090.

[22] Garcia-Saez, I., Hopkins, J., Papamicael, C., Franceschini, N., Amicosante, G., Rossolini, G. M., Galleni, M., Frere, J. M., and Dideberg, O. (2003) The 1.5-A structure of Chryseobacterium meningosepticum zinc beta-lactamase in complex with the inhibitor, D-captopril, *J Biol Chem 278*, 23868-23873.

[23] Kurosaki, H., Yamaguchi, Y., Yasuzawa, H., Jin, W., Yamagata, Y., and Arakawa, Y. (2006) Probing, inhibition, and crystallographic characterization of metallo-beta-lactamase (IMP-1) with fluorescent agents containing dansyl and thiol groups, *ChemMedChem 1*, 969-972.

[24] Yamaguchi, Y., Jin, W., Matsunaga, K., Ikemizu, S., Yamagata, Y., Wachino, J., Shibata, N., Arakawa, Y., and Kurosaki, H. (2007) Crystallographic investigation of the inhibition mode of a VIM-2 metallo-beta-lactamase from Pseudomonas aeruginosa by a mercaptocarboxylate inhibitor, *J Med Chem 50*, 6647-6653.

[25] Wachino, J., Yamaguchi, Y., Mori, S., Kurosaki, H., Arakawa, Y., and Shibayama, K. (2013) Structural insights into the subclass B3 metallo-beta-lactamase SMB-1 and the mode of inhibition by the common metallo-beta-lactamase inhibitor mercaptoacetate, *Antimicrob Agents Chemother 57*, 101-109.

[26] Nauton, L., Kahn, R., Garau, G., Hernandez, J. F., and Dideberg, O. (2008) Structural insights into the design of inhibitors for the L1 metallo-beta-lactamase from Stenotrophomonas maltophilia, *J Mol Biol 375*, 257-269.

[27] Lassaux, P., Hamel, M., Gulea, M., Delbruck, H., Mercuri, P. S., Horsfall, L., Dehareng, D., Kupper, M., Frère, J. M., Hoffmann, K., Galleni, M., and Bebrone, C. (2010) Mercaptophosphonate compounds as broad-spectrum inhibitors of the metallo-beta-lactamases, *J Med Chem 53*, 4862-4876.

[28] Toney, J. H., Cleary, K. A., Hammond, G. G., Yuan, X., May, W. J., Hutchins, S. M., Ashton, W. T., and Vanderwall, D. E. (1999) Structure-activity relationships of biphenyl tetrazoles as metallo-beta-lactamase inhibitors, *Bioorg Med Chem Lett 9*, 2741-2746.

[29] Hiraiwa, Y., Saito, J., Watanabe, T., Yamada, M., Morinaka, A., Fukushima, T., and Kudo, T. (2014) X-ray crystallographic analysis of IMP-1 metallo-beta-lactamase complexed with a 3-aminophthalic acid derivative, structure-based drug design, and synthesis of 3,6-disubstituted phthalic acid derivative inhibitors, *Bioorg Med Chem Lett 24*, 4891-4894.

[30] Horsfall, L. E., Garau, G., Lienard, B. M., Dideberg, O., Schofield, C. J., Frère, J. M., and Galleni, M. (2007) Competitive inhibitors of the CphA metallo-beta-lactamase from Aeromonas hydrophila, *Antimicrob Agents Chemother 51*, 2136-2142.

[31] Toney, J. H., Fitzgerald, P. M., Grover-Sharma, N., Olson, S. H., May, W. J., Sundelof, J. G., Vanderwall, D. E., Cleary, K. A., Grant, S. K., Wu, J. K., Kozarich, J. W., Pompliano, D. L., and Hammond, G. G. (1998) Antibiotic sensitization using biphenyl tetrazoles as potent inhibitors of Bacteroides fragilis metallo-beta-lactamase, *Chem Biol 5*, 185-196.

[32] Docquier, J. D., Benvenuti, M., Calderone, V., Stoczko, M., Menciassi, N., Rossolini, G. M., and Mangani, S. (2010) High-resolution crystal structure of the subclass B3 metallo-beta-lactamase BJP-1: rational basis for substrate specificity and interaction with sulfonamides, *Antimicrob Agents Chemother 54*, 4343-4351.

27

[33] Brem, J., Cain, R., Cahill, S., McDonough, M. A., Clifton, I. J., Jimenez-Castellanos, J. C., Avison, M. B., Spencer, J., Fishwick, C. W., and Schofield, C. J. (2016) Structural basis of metallo-beta-lactamase, serine-beta-lactamase and penicillin-binding protein inhibition by cyclic boronates, *Nat Commun 7*, 12406.

[34] Calvopina, K., Hinchliffe, P., Brem, J., Heesom, K. J., Johnson, S., Cain, R., Lohans, C. T., Fishwick, C. W. G., Schofield, C. J., Spencer, J., and Avison, M. B. (2017) Structural/mechanistic insights into the efficacy of nonclassical beta-lactamase inhibitors against extensively drug resistant Stenotrophomonas maltophilia clinical isolates, *Mol Microbiol 106*, 492-504.

[35] Jacobsen, J. A., Major Jourden, J. L., Miller, M. T., and Cohen, S. M. (2010) To bind zinc or not to bind zinc: an examination of innovative approaches to improved metalloproteinase inhibition, *Biochim Biophys Acta 1803*, 72-94.

[36] Temperini, C., Innocenti, A., Guerri, A., Scozzafava, A., Rusconi, S., and Supuran, C. T. (2007) Phosph(on)ate as a zinc-binding group in metalloenzyme inhibitors: X-ray crystal structure of the antiviral drug foscarnet complexed to human carbonic anhydrase I, *Bioorg Med Chem Lett 17*, 2210-2215.

[37] Tronrud, D. E., Monzingo, A. F., and Matthews, B. W. (1986) Crystallographic structural analysis of phosphoramidates as inhibitors and transition-state analogs of thermolysin, *Eur J Biochem 157*, 261-268.

[38] Maveyraud, L., Pratt, R. F., and Samama, J. P. (1998) Crystal structure of an acylation transition-state analog of the TEM-1 beta-lactamase. Mechanistic implications for class A beta-lactamases, *Biochemistry 37*, 2622-2628.

[39] Chen, C. C., Rahil, J., Pratt, R. F., and Herzberg, O. (1993) Structure of a phosphonate-inhibited beta-lactamase. An analog of the tetrahedral transition state/intermediate of beta-lactam hydrolysis, *J Mol Biol 234*, 165-178.

[40] Yang, K. W., Feng, L., Yang, S. K., Aitha, M., LaCuran, A. E., Oelschlaeger, P., and Crowder, M. W. (2013) New beta-phospholactam as a carbapenem transition state analog: Synthesis of a broad-spectrum inhibitor of metallo-beta-lactamases, *Bioorg Med Chem Lett 23*, 5855-5859.

[41] Lee, M., Hesek, D., and Mobashery, S. (2005) A practical synthesis of nitrocefin, *J Org Chem 70*, 367-369.

[42] Labbé, G., Krismanich, A. P., de Groot, S., Rasmusson, T., Shang, M., Brown, M. D., Dmitrienko, G. I., and Guillemette, J. G. (2012) Development of metal-chelating inhibitors for the Class II fructose 1,6-bisphosphate (FBP) aldolase, *J Inorg Biochem 112*, 49-58.

[43] Li, G. B., Brem, J., Lesniak, R., Abboud, M. I., Lohans, C. T., Clifton, I. J., Yang, S. Y., Jimenez-Castellanos, J. C., Avison, M. B., Spencer, J., McDonough, M. A., and Schofield, C. J. (2017) Crystallographic analyses of isoquinoline complexes reveal a new mode of metallo-beta-lactamase inhibition, *Chem Commun (Camb) 53*, 5806-5809.

[44] King, A. M., Reid-Yu, S. A., Wang, W., King, D. T., De Pascale, G., Strynadka, N. C., Walsh, T. R., Coombes, B. K., and Wright, G. D. (2014) Aspergillomarasmine A overcomes metallo-beta-lactamase antibiotic resistance, *Nature 510*, 503-506.

[45] Crossman, L. C., Gould, V. C., Dow, J. M., Vernikos, G. S., Okazaki, A., Sebaihia, M., Saunders, D., Arrowsmith, C., Carver, T., Peters, N., Adlem, E., Kerhornou, A., Lord, A., Murphy, L., Seeger, K., Squares, R., Rutter, S., Quail, M. A., Rajandream, M.-A., Harris, D., Churcher, C., Bentley, S. D., Parkhill, J., Thomson, N. R., and Avison, M. B. (2008) The complete genome, comparative and functional analysis of Stenotrophomonas maltophiliareveals an organism heavily shielded by drug resistance determinants, *Genome Biology 9*, 1-13.

[46] Gould, V. C., and Avison, M. B. (2006) SmeDEF-mediated antimicrobial drug resistance in Stenotrophomonas maltophilia clinical isolates having defined phylogenetic relationships, *J Antimicrob Chemother 57*, 1070-1076.

[47] Gould, V. C., Okazaki, A., and Avison, M. B. (2013) Coordinate hyperproduction of SmeZ and SmeJK efflux pumps extends drug resistance in Stenotrophomonas maltophilia, *Antimicrob Agents Chemother 57*, 655-657.

28

[48] CLSI. *Performance Standards for Antimicrobial Susceptibility Testing: Twenty-fourth Informational Supplement M100-S24. CLSI, Wayne, 433 PA, USA, 2014.*

[49] Dayeh, V. R., Schirmer, K., Lee, L. E. J., and Bols, N. C. (2003) The use of fish-derived cell lines for investigation of environmental contaminants. In: Current Protocols in Toxicology. Wiley, New York, pp. 1–17 (Unit 1.5). *In: Current Protocols in Toxicology. Wiley, New York, pp. 1–17 (Unit 1.5).*

[50] Ganassin, R. C., Schirmer, K., and Bols, N. C. (2000) Methods for the use of fish cell and tissue cultures as model systems in basic and toxicology research. In: Ostrander, G.K. (Ed.), The Laboratory Fish. Academic Press, San Diego, pp. 631–651., *In: Ostrander, G.K. (Ed.), The Laboratory Fish. Academic Press, San Diego, pp. 631–651.*

[51] Ullah, J. H., Walsh, T. R., Taylor, I. A., Emery, D. C., Verma, C. S., Gamblin, S. J., and Spencer, J. (1998) The crystal structure of the L1 metallo-beta-lactamase from Stenotrophomonas maltophilia at 1.7 A resolution, *J Mol Biol 284*, 125-136.

[52] van Berkel, S. S., Brem, J., Rydzik, A. M., Salimraj, R., Cain, R., Verma, A., Owens, R. J., Fishwick, C. W., Spencer, J., and Schofield, C. J. (2013) Assay platform for clinically relevant metallo-beta-lactamases, *J Med Chem 56*, 6945-6953.

[53] Ghavami, A., Labbé, G., Brem, J., Goodfellow, V. J., Marrone, L., Tanner, C. A., King, D. T., Lam, M., Strynadka, N. C., Pillai, D. R., Siemann, S., Spencer, J., Schofield, C. J., and Dmitrienko, G. I. (2015) Assay for drug discovery: Synthesis and testing of nitrocefin analogues for use as beta-lactamase substrates, *Anal Biochem 486*, 75-77.

[54] Morrison, J. F., and Walsh, C. T. (1988) The behavior and significance of slow-binding enzyme inhibitors, *Adv Enzymol Relat Areas Mol Biol 61*, 201-301.

[55] Goličnik, M., and Stojan, J. (2004) Slow-binding inhibition: A theoretical and practical course for students, *Biochem Mol Biol Educ 32*, 228-235.

[56] Kabsch, W. (2010) Xds, *Acta Crystallogr D Biol Crystallogr 66*, 125-132.

[57] Evans, P. R. (2011) An introduction to data reduction: space-group determination, scaling and intensity statistics, *Acta Crystallogr D Biol Crystallogr 67*, 282-292.

[58] McCoy, A. J., Grosse-Kunstleve, R. W., Adams, P. D., Winn, M. D., Storoni, L. C., and Read, R. J. (2007) Phaser crystallographic software, *J Appl Crystallogr 40*, 658-674.

[59] Emsley, P., Lohkamp, B., Scott, W. G., and Cowtan, K. (2010) Features and development of Coot, *Acta Crystallogr D Biol Crystallogr 66*, 486-501.

[60] Adams, P. D., Afonine, P. V., Bunkoczi, G., Chen, V. B., Davis, I. W., Echols, N., Headd, J. J., Hung, L. W., Kapral, G. J., Grosse-Kunstleve, R. W., McCoy, A. J., Moriarty, N. W., Oeffner, R., Read, R. J., Richardson, D. C., Richardson, J. S., Terwilliger, T. C., and Zwart, P. H. (2010) PHENIX: a comprehensive Python-based system for macromolecular structure solution, *Acta Crystallogr D Biol Crystallogr 66*, 213-221.

[61] Chen, V. B., Arendall, W. B., 3rd, Headd, J. J., Keedy, D. A., Immormino, R. M., Kapral, G. J., Murray, L. W., Richardson, J. S., and Richardson, D. C. (2010) MolProbity: all-atom structure validation for macromolecular crystallography, *Acta Crystallogr D Biol Crystallogr 66*, 12-21.

[62] Roll, D. M., Yang, Y., Wildey, M. J., Bush, K., and Lee, M. D. (2010) Inhibition of metallo-beta-lactamases by pyridine monothiocarboxylic acid analogs, *J Antibiot (Tokyo) 63*, 255-257.

[63] Siemann, S., Brewer, D., Clarke, A. J., Dmitrienko, G. I., Lajoie, G., and Viswanatha, T. (2002) IMP-1 metallo-beta-lactamase: effect of chelators and assessment of metal requirement by electrospray mass spectrometry, *Biochim Biophys Acta 1571*, 190-200.

[64] Chen, A. Y., Thomas, P. W., Stewart, A. C., Bergstrom, A., Cheng, Z., Miller, C., Bethel, C. R., Marshall, S. H., Credille, C. V., Riley, C. L., Page, R. C., Bonomo, R. A., Crowder, M. W., Tierney, D. L., Fast, W., and Cohen, S. M. (2017) Dipicolinic Acid Derivatives as Inhibitors of New Delhi Metallo-beta-lactamase-1, *J Med Chem 60*, 7267-7283.

[65] Meini, M.-R., Llarrull, L. I., and Vila, A. J. (2014) Evolution of Metallo-β-lactamases: Trends Revealed by Natural Diversity and in vitro Evolution, *Antibiotics 3*, 285-316.

29

[66] Copeland, R. A. (2005) Evaluation of enzyme inhibitors in drug discovery. A guide for medicinal chemists and pharmacologists, *Methods Biochem Anal 46*, 1-265.

[67] Siemann, S., Clarke, A. J., Viswanatha, T., and Dmitrienko, G. I. (2003) Thiols as classical and slow-binding inhibitors of IMP-1 and other binuclear metallo-beta-lactamases, *Biochemistry 42*, 1673-1683.

[68] Badarau, A., Llinas, A., Laws, A. P., Damblon, C., and Page, M. I. (2005) Inhibitors of metallo-beta-lactamase generated from beta-lactam antibiotics, *Biochemistry 44*, 8578-8589.

[69] Mondal, J., Morrone, J. A., and Berne, B. J. (2013) How hydrophobic drying forces impact the kinetics of molecular recognition, *Proc Natl Acad Sci U S A 110*, 13277-13282.

[70] Copeland, R. A. (2010) The dynamics of drug-target interactions: drug-target residence time and its impact on efficacy and safety, *Expert Opin Drug Discov 5*, 305-310.

[71] Copeland, R. A., Pompliano, D. L., and Meek, T. D. (2006) Drug-target residence time and its implications for lead optimization, *Nat Rev Drug Discov 5*, 730-739.

[72] Dahl, G., and Akerud, T. (2013) Pharmacokinetics and the drug-target residence time concept, *Drug Discov Today 18*, 697-707.

[73] Walkup, G. K., You, Z., Ross, P. L., Allen, E. K., Daryaee, F., Hale, M. R., O'Donnell, J., Ehmann, D. E., Schuck, V. J., Buurman, E. T., Choy, A. L., Hajec, L., Murphy-Benenato, K., Marone, V., Patey, S. A., Grosser, L. A., Johnstone, M., Walker, S. G., Tonge, P. J., and Fisher, S. L. (2015) Translating slow-binding inhibition kinetics into cellular and in vivo effects, *Nat Chem Biol 11*, 416-423.

[74] Papagiannitsis, C. C., Izdebski, R., Baraniak, A., Fiett, J., Herda, M., Hrabak, J., Derde, L. P., Bonten, M. J., Carmeli, Y., Goossens, H., Hryniewicz, W., Brun-Buisson, C., Gniadkowski, M., Mosar Wp, W. P., groups, W. P. s., Mosar Wp, W. P., and groups, W. P. s. (2015) Survey of metallo-beta-lactamase-producing Enterobacteriaceae colonizing patients in European ICUs and rehabilitation units, 2008-11, *J Antimicrob Chemother 70*, 1981-1988.

[75] EUCAST. *The European Committee on Antimicrobial Susceptibility Testing. Breakpoint tables for interpretation of MICs and zone diameters. Version 7.1, 2017.* http://www.eucast.org.

[76] Walsh, F. (2007) Doripenem: A new carbapenem antibiotic a review of comparative antimicrobial and bactericidal activities, *Ther Clin Risk Manag 3*, 789-794.

[77] Looney, W. J., Narita, M., and Muhlemann, K. (2009) Stenotrophomonas maltophilia: an emerging opportunist human pathogen, *Lancet Infect Dis 9*, 312-323.

[78] Waters, V., Yau, Y., Prasad, S., Lu, A., Atenafu, E., Crandall, I., Tom, S., Tullis, E., and Ratjen, F. (2011) Stenotrophomonas maltophilia in cystic fibrosis: serologic response and effect on lung disease, *Am J Respir Crit Care Med 183*, 635-640.

[79] Freedman, L. D., and Doak, G. O. (1957) The Preparation And Properties Of Phosphonic Acids, *Chemical Reviews 57*, 479-523.

[80] Yu, H., Kuhne, R., Ebert, R. U., and Schuurmann, G. (2010) Comparative analysis of QSAR models for predicting pK(a) of organic oxygen acids and nitrogen bases from molecular structure, *J Chem Inf Model 50*, 1949-1960.

[81] Giamarellou, H., and Antoniadou, A. (2001) Antipseudomonal antibiotics, *Med Clin North Am 85*, 19-42, v.

[82] Garuti, L., Ferranti, A., Roberti, M., Katz, E., Budriesi, R., and Chiarini, A. (1992) Synthesis and biological evaluation of some new phosphonates, *Pharmazie 47*, 295-297.

[83] Martinez, C. R., and Iverson, B. L. (2012) Rethinking the term "pi-stacking", *Chemical Science 3*, 2191-2201.

[84] Gardonio, D., and Siemann, S. (2009) Chelator-facilitated chemical modification of IMP-1 metallo-beta-lactamase and its consequences on metal binding, *Biochem Biophys Res Commun 381*, 107-111.

[85] Toney, J. H., Hammond, G. G., Fitzgerald, P. M., Sharma, N., Balkovec, J. M., Rouen, G. P., Olson, S. H., Hammond, M. L., Greenlee, M. L., and Gao, Y. D. (2001) Succinic acids as potent inhibitors of plasmid-borne IMP-1 metallo-beta-lactamase, *J Biol Chem 276*, 31913-31918.

[86] Payne, D. J., Hueso-Rodríguez, J. A., Boyd, H., Concha, N. O., Janson, C. A., Gilpin, M., Bateson, J. H., Cheever, C., Niconovich, N. L., Pearson, S., Rittenhouse, S., Tew, D., Díez, E., Pérez, P., de la Fuente, J., Rees, M., and Rivera-Sagredo, A. (2002) Identification of a Series of Tricyclic Natural Products as Potent Broad-Spectrum Inhibitors of Metallo-β-Lactamases, *Antimicrobial Agents and Chemotherapy 46*, 1880-1886.

[87] Costello, A., Periyannan, G., Yang, K. W., Crowder, M. W., and Tierney, D. L. (2006) Site-selective binding of Zn(II) to metallo-beta-lactamase L1 from Stenotrophomonas maltophilia, *J Biol Inorg Chem 11*, 351-358.

[88] Griffin, D. H., Richmond, T. K., Sanchez, C., Moller, A. J., Breece, R. M., Tierney, D. L., Bennett, B., and Crowder, M. W. (2011) Structural and kinetic studies on metallo-beta-lactamase IMP-1, *Biochemistry 50*, 9125-9134.

[89] Calvopina, K., Umland, K. D., Rydzik, A. M., Hinchliffe, P., Brem, J., Spencer, J., Schofield, C. J., and Avison, M. B. (2016) Sideromimic Modification of Lactivicin Dramatically Increases Potency against Extensively Drug-Resistant Stenotrophomonas maltophilia Clinical Isolates, *Antimicrob Agents Chemother 60*, 4170-4175.

31

Table 1. IC$_{50}$ values for PMPCs against representative MBLs with nitrocefin substrate

Inhibitor	IC$_{50}$ (µM)			
	VIM-2	NDM-1	IMP-1	L1
1	32.2	>100	>100	>100
2	>100	>100	>100	>100
3a	1.29	0.374	3.88	1.48
3b	1.90	0.322	7.20	2.05
3c	0.464	0.306	2.91	1.57
4	171	>1000	>100	>1000

1
2
3
4
5
6
7
8
9
10
11
12
13
14
15
16
17
18
19
20
21
22
23
24
25
26
27
28
29
30
31
32
33
34
35
36
37
38
39
40
41
42
43
44
45
46
47
48
49
50
51
52
53
54
55
56
57
58
59
60

Table 2. Inhibition constants for PMPCs against MBLs

inhibitor	K_i (μM)			
	VIM-2	NDM-1	IMP-1	L1
3a	0.5 ± 0.05	0.07 ± 0.01	1 ± 0.2	0.5 ± 0.1
3b	0.6 ± 0.04	0.07 ± 0.01	2 ± 0.1	0.4 ± 0.1
3c	0.04 ± 0.009	0.03 ± 0.003	0.4 ± 0.2	0.4 ± 0.1

Table 3. Potentiation of Meropenem Activity Against Recombinant B1 MBL-Producing Bacteria by PMPCs

Strain	MBL[*]	Meropenem MIC (mg L^{-1}) in absence of inhibitor	Meropenem MIC (mg L^{-1}) in the presence of 3a at stated concentration		
			10 mg L^{-1}	50 mg L^{-1}	100 mg L^{-1}
E. coli MG1655	Vector only	<0.25	<0.25	<0.25	<0.25
E. coli MG1655	IMP-1	16	16	2	<0.25
E. coli MG1655	VIM-1	4	4	2	<0.25
E. coli MG1655	NDM-1	>256	>256	128	8
Klebsiella pneumoniae Ecl8	NDM-1	>256	>256	64	4
Citrobacter freundii D571	NDM-1	32	32	8	2
Enterobacter aerogenes 15-8358A	NDM-1	64	64	16	1

[*]MBL expressed from its native promoter, encoded on the pSU18 vector

Table 4. Potentiation of Meropenem activity against MBL-producing Clinical Strains by 3a

Strain	Resistance determinant (MBL/SBL)	Meropenem MIC (mg L^{-1}) in absence of inhibitor	Meropenem MIC (mg L^{-1}) in the presence of 3a at stated concentration					
			4 mg L^{-1}	8 mg L^{-1}	16 mg L^{-1}	32 mg L^{-1}	64 mg L^{-1}	128 mg L^{-1}
P. aeruginosa #UWB41	VIM-2	128	64	64	64	32	4	0.5
P. putida #UWB24	VIM-2	64	64	64	64	32	8	2
E. coli #UWB75	NDM-1 / CTX-M-15	128	128	128	64	16	1	<0.25
P. aeruginosa #UWB78	VIM-2	64	64	64	64	32	8	4
S. maltophilia K279a	L1, L2	16	16	16	16	16	8	4
S. maltophilia Kami32	L1, L2	16	16	16	16	16	8	8
S. maltophilia JKWZP	L1, L2	32	32	32	32	32	16	8
K. pneumoniae #UWB116	NDM-1	32	16	8	4	0.25	<0.125	<0.125
E. coli #UWB93	IMP-1 / CTX-M-15	4	4	4	4	2	0.5	0.25

35

1
2
3
4
5
6
7
8
9
10
11
12
13
14
15
16
17
18
19
20
21
22
23
24
25
26
27
28
29
30
31
32
33
34
35
36
37
38
39
40
41
42
43
44
45
46
47
48
49
50
51
52
53
54
55
56
57
58
59
60

For Table of Contents Use Only